Available online at www.sciencedirect.com
ScienceDirect
Journal of Sound and Vibration 321 (2009) 471–491
JOURNAL OF SOUND AND VIBRATION
www.elsevier.com/locate/jsvi

Two tracking control problems applied to damping nonlinear vehicle vibrations

E.M. ElBeheiry*

Department of Mechanical Engineering, College of Engineering, Qassim University, P.O. Box 6677, 51452 Buriada, Qassim, Saudi Arabia

Received 15 January 2008; received in revised form 20 September 2008; accepted 23 September 2008
Handling Editor: M.P. Cartmell
Available online 31 October 2008

Abstract

A global control strategy of linear and nonlinear control methods is developed for application to the design of hydraulic suspensions in ground vehicles. A nonlinear, three-dimensional passenger car model of 7-dof is used to investigate vehicle ride capabilities with hydraulic actuators employed as active suspension elements. The design procedure starts with the application of an optimal control method of multiple-structure constraints to the optimization of suspension performance in the absence of system nonlinearities. Hence, the strong nonlinearity of hydraulic actuators is considered, and the optimal linear solutions are implemented as reference values to be asymptotically tracked. Two contrasting nonlinear control methods, called input–output linearization and sliding mode control, are used to achieve the asymptotic tracking problem in the presence of Coulomb friction and model uncertainties. Digital simulation shows that the input–output controller is effective as long as the suspension is frictionless and the system knowledge is perfect. Conversely, the robustness of the sliding mode controller makes it capable of providing good tracking even in cases of model uncertainty. The whole design procedure is demonstrated with numerical examples showing its significance. The procedure also allows for the simultaneous design of optimal passive suspension elements to be mechanized in parallel with the hydraulic actuators in order to increase suspension reliability.

1. Introduction

Active suspensions in ground vehicles have been the focus of a great deal of attention in the last three decades [1]. Their performance superiority over classical (passive) suspensions has been accepted as fact. This superiority is not only limited to the vehicle ride quality [2–4] but is also extendable to the vehicle handling capabilities [5]. A lot of effort has been made to commercialize fully active suspensions, but they are still unusual in mass-production vehicles in low-price markets. This can be attributed to their high cost and complexity of hardware and signal processing. The term "fully active" suspension means that a broadband (force generator) actuator of greater than 8 Hz is mechanized into each suspension unit of the vehicle.

*Tel.: +966 558 778 640; fax: +966 638 000 50x5311.
E-mail addresses: elbeheiry@yahoo.com, elbeheiry@hotmail.com.

0022-460X/$ - see front matter © 2008 Elsevier Ltd. All rights reserved.
doi:10.1016/j.jsv.2008.09.043

The actuator itself could be either a pneumatic, hydraulic, electromechanical, or magnetic force generator, depending on the vehicle application.

The main deficiencies of hydraulic actuators when applied to active vehicle suspensions lie in their strong nonlinearity, Coulomb friction, and parameter uncertainty. These deficiencies, if not appropriately handled, can deteriorate the performance of active vehicle suspensions. Most nonlinear control design methods depend on having a reference system model to be tracked by the nonlinear controller. This is a difficult task to accomplish in the majority of engineering applications, notwithstanding the additional complexities brought about by the above mentioned deficiencies. In the field of active vehicle suspensions, a good resolution to this problem has been presented in Ref. [6]. The authors suggested the use of a skyhook damping performance as a means to have a reference (linearized) best-performance system model. They used a quarter-car model with two-degrees of freedom in order to explore their concept and generated a robust nonlinear hydraulic force to track the performance of the skyhook damping force, chosen on the basis of a linear simplified quarter-car model. However, the authors did not present any optimization criteria for choosing the best skyhook damping values in terms of the performance measures of vehicle suspensions. This concept is appropriate for simple one-dimensional vehicle models, but it needs to be further developed before application to a realistic vehicle model, which is partially the topic of this article. Dealing with uncertainties in active suspension applications would require either robust control designs [7,8] or adaptive control techniques [9,10]. Switching at the sliding surface of the control law represents a significant source of chattering; this degrades performance and may cause instability due to the high-frequency resonance of the fluid column in hydraulic actuators. On the other hand, many adaptive techniques require modifications to guarantee boundedness of the estimates, making it difficult to guarantee transient tracking accuracy; asymptotic tracking may be lost even when external disturbances do not exist [11]. Some other adaptive techniques do not necessitate justification of the condition of bounded estimations [12]. This makes them more suitable for many practical applications.

A fuzzy logic system, described by Campos in Ref. [13], is used to estimate the nonlinear hydraulic strut dynamics. The fuzzy logic system was adapted to estimate the unknown hydraulic dynamics and to provide the backstepping loop with the desired servovalve positioning so that the scheme becomes adaptive, guaranteeing bounded tracking errors and parameter estimates. Huang and Chao [14] presented a model-free fuzzy control algorithm for the design of a controller for achieving vibration isolation, rather than resorting to the classical model-based control design. Kadissi [15] relaxed one important assumption that has always been considered in the literature; the chamber volume of the hydraulic actuator is usually assumed to be constant, when in fact the volume varies with the piston motion. Thus, an additional nonlinear term was added to the classic model, and the backstepping technique was used as a powerful nonlinear approach capable of overwhelming all those facets. Renn and Wu [16] reported that the performance of neural network controller is somewhat better than that obtained from the PID controller for active vehicle suspensions. Their study was verified theoretically and experimentally.

In this paper, reference best-performance skyhook damping forces are obtained on a comprehensive three-dimensional vehicle model by the application of a multiple control structure constraints method as a sub-optimal regulator design method. Then, two contrasting nonlinear controllers, an input–output controller and a sliding mode controller, are designed to track the optimized skyhook damping forces. The combination of linear and nonlinear control design methods represents a hybrid approach to control the generated hydraulic forces of fully active suspensions in ground vehicles.

2. Vehicle model

Accurate modeling of vehicle dynamics is not an easy task, especially when handling actions like turning and braking. The vehicle in Fig. 1 is assumed to travel in a straight line at a constant travel speed without any kind of braking and cornering actions. Thus, the resulting total number of degrees of freedom can be reasonably confined to 7, three of them for heave, roll, and pitch motions of the sprung mass and four for the vertical motion of the four tires. Dynamics of the four hydraulic force generators are considered as the only source of nonlinearity in the resulting nonlinear 7-dof model.

It has been accepted in the vehicle research community that, in the 7-dof vehicle model, coupling between the two rear wheels is of negligible effect and can be cancelled. This fact only holds true as long as the purpose

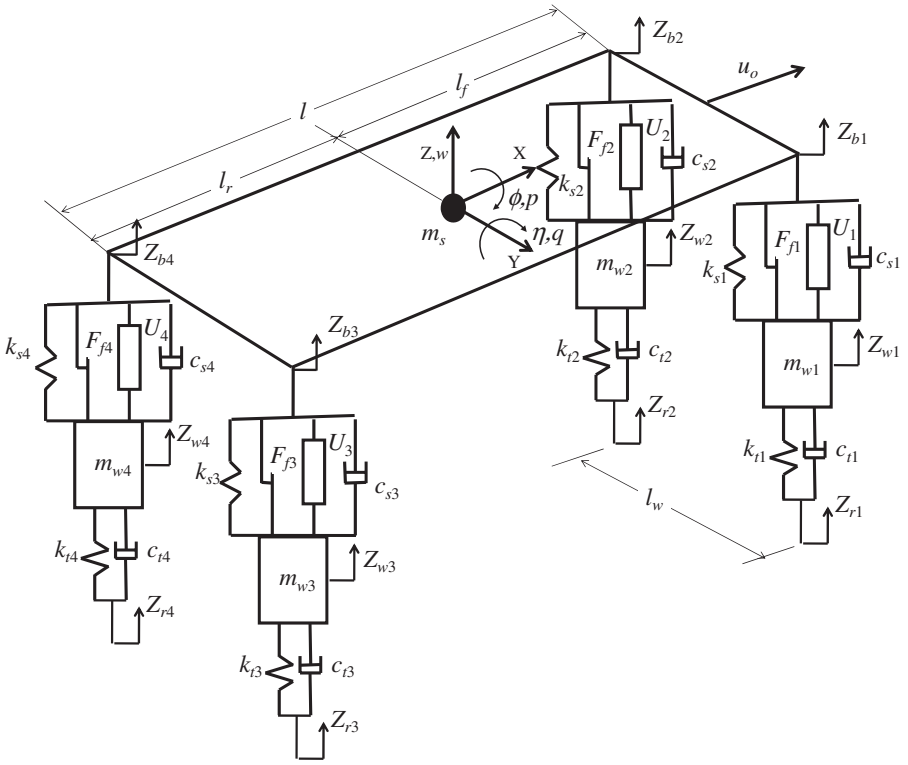

Fig. 1. Schematics of a three-dimensional vehicle model.

of the study is to investigate vehicle ride quality against road roughness undulation, e.g., random vehicle vibrations due to stochastic road inputs, which are considered in this study. Moreover, vehicle handling actions like braking and cornering are out of scope of this study. The nonlinear 7-dof model that is implemented in this study only focuses on hydraulic actuator strong nonlinearities, coulomb friction, and parameter uncertainty. Other important nonlinearities due to suspension kinematics and geometry, pneumatic tires and vehicle structure have all been ignored. In fact, considering all those sources of nonlinearities would prevent us from being able to understand the performance potentials and physical insights of hydraulic actuators.

In the simplified nonlinear 7-dof model that is considered here, no explicit description will be given to variables related to the dynamics of ground reaction forces, the motion of the car mass center, etc. This is because, with the assumptions that we made above, the static and dynamic parts of these variables due to gravitational forces, braking, cornering, sprung mass load transfer have been all neglected. Thus, they do not contribute to the model of the vibratory motion of the vehicle. Only small deviations of some of these variables from the equilibrium state due to road undulation are considered. For example, the normal tire forces are only considered as functions of their deflections and the rate of deflections due to stochastic road inputs. The other tire forces are all zeros as long as we assume that no cornering and braking actions take place while the vehicle is heading in a straight line with a constant speed. The kinematic motion of the car's center of mass is cancelled under the same sort of assumptions. In other words, the sprung mass is regarded as a symmetric rigid body having its roll axis coincide with its longitudinal axis of symmetry. Readers who are interested in a full description of these variables in cases of combined braking and cornering actions should refer to ElBeheiry et al. [5].

Under the assumptions made above, Fig. 1 shows the XYZ-axis system that is attached to the vehicle center of gravity where the forward travel speed is u_o, the heave motion is Z, the heave rate is w, the pitch angle is η, the pitch rate is q, the roll angle is ϕ, and the roll rate is p. m_s is the sprung mass, m_{wi}, $i = 1,\ldots,4$, are masses of the tires, I_x and I_z are the vehicle polar moment of inertia about the longitudinal and vertical axes,

respectively. l_w is the wheel base, l_f is the distance from the front axle to the vehicle c.o.g., l_r is the distance from the rear axle to the vehicle c.o.g., and $l = l_f + l_r$ is the distance between the front and rear axles. c_{si} and K_{si}, $i = 1,\ldots,4$, are the passive suspension damping and stiffness, respectively. c_{ti} and k_{ti}, $i = 1,\ldots,4$, are the tire damping and stiffness coefficients, respectively. Z_{ri}, $i = 1,\ldots,4$, are the stochastic road inputs, Z_{wi}, $i = 1,\ldots,4$, are the wheel displacements, Z_{bi}, $i = 1,\ldots,4$, are the sprung mass displacements at the suspension connections, Z_{si}, $i = 1,\ldots,4$, are the suspension deflections, Z_{ti}, $i = 1,\ldots,4$, are the tire deflections, and a_{wi}, $i = 1,\ldots,4$, are the wheel accelerations. Note here that, according to the assumptions of the nonlinear 7-dof, Z, η and ϕ represent the most important degrees of freedom of the sprung mass.

The tire-suspension assembly is schematically shown at the vehicle's four corners in Fig. 1. The tire forces are all defined in the tire local axis system. The normal (vertical) tire forces are F_{ti}, $i = 1,\ldots,4$,. F_{si}, $i = 1,\ldots,4$, are suspension-generated forces applied to both the sprung and the unsprung masses. F_{fi}, $i = 1,\ldots,4$, are suspension frictional forces, and U_i, $i = 1,\ldots,4$, are generated hydraulic actuator forces.

The model's equations of motion are

$$m_s\dot{w} = -F_{s1} - F_{s2} - F_{s3} - F_{s4}, \tag{1}$$

$$I_x\dot{p} = -\left(\frac{l_w}{2}\right)\begin{vmatrix} 1 & 1 \\ (F_{s2}+F_{s4}) & (F_{s1}+F_{s3}) \end{vmatrix}, \tag{2}$$

$$I_y\dot{q} = -\begin{vmatrix} l_f & l_r \\ (F_{s3}+F_{s4}) & (F_{s1}+F_{s2}) \end{vmatrix}, \tag{3}$$

$$m_{w1}a_{w1} = +F_{s1} - F_{t1}, \quad m_{w2}a_{w2} = +F_{s2} - F_{t2}, \tag{4,5}$$

$$m_{w3}a_{w3} = +F_{s3} - F_{t3}, \quad m_{w4}a_{w4} = +F_{s4} - F_{t4}, \tag{6,7}$$

where the tire forces due to their deflections and rate of deflections are given by

$$\begin{pmatrix} F_{t1} \\ F_{t2} \\ F_{t3} \\ F_{t4} \end{pmatrix} = \begin{pmatrix} k_{t1} & 0 & 0 & 0 \\ 0 & k_{t2} & 0 & 0 \\ 0 & 0 & k_{t3} & 0 \\ 0 & 0 & 0 & k_{t4} \end{pmatrix}\begin{pmatrix} Z_{t1} \\ Z_{t2} \\ Z_{t3} \\ Z_{t4} \end{pmatrix} + \begin{pmatrix} c_{t1} & 0 & 0 & 0 \\ 0 & c_{t2} & 0 & 0 \\ 0 & 0 & c_{t3} & 0 \\ 0 & 0 & 0 & c_{t4} \end{pmatrix}\begin{pmatrix} \dot{Z}_{t1} \\ \dot{Z}_{t2} \\ \dot{Z}_{t3} \\ \dot{Z}_{t4} \end{pmatrix}, \tag{8}$$

and the suspension forces due to their deflections and rate of deflections are given by

$$\begin{pmatrix} F_{s1} \\ F_{s2} \\ F_{s3} \\ F_{s4} \end{pmatrix} = \begin{pmatrix} k_{s1} & 0 & 0 & 0 \\ 0 & k_{s2} & 0 & 0 \\ 0 & 0 & k_{s3} & 0 \\ 0 & 0 & 0 & k_{s4} \end{pmatrix}\begin{pmatrix} Z_{s1} \\ Z_{s2} \\ Z_{s3} \\ Z_{s4} \end{pmatrix} + \begin{pmatrix} c_{s1} & 0 & 0 & 0 \\ 0 & c_{s2} & 0 & 0 \\ 0 & 0 & c_{s3} & 0 \\ 0 & 0 & 0 & c_{s4} \end{pmatrix}\begin{pmatrix} \dot{Z}_{s1} \\ \dot{Z}_{s2} \\ \dot{Z}_{s3} \\ \dot{Z}_{s4} \end{pmatrix} + \begin{pmatrix} U_1 - F_{f1} \\ U_2 - F_{2l} \\ U_3 - F_{f3} \\ U_4 - F_{f4} \end{pmatrix}. \tag{9}$$

In the last equations, the tire and suspension deflections can be calculated by

$$Z_{ti} = Z_{wi} - Z_{ri}, \quad Z_{si} = Z_{bi} - Z_{wi}, \ \ i = 1, 2, \ldots, 4, \tag{10}$$

or in matrix form:

$$\begin{pmatrix} Z_{s1} \\ Z_{s2} \\ Z_{s3} \\ Z_{s4} \end{pmatrix} = \begin{pmatrix} Z_{b1} \\ Z_{b2} \\ Z_{b3} \\ Z_{b4} \end{pmatrix} - \begin{pmatrix} Z_{w1} \\ Z_{w2} \\ Z_{w3} \\ Z_{w4} \end{pmatrix} = \begin{pmatrix} 1 & -l_f & -l_w/2 \\ 1 & -l_f & +l_w/2 \\ 1 & +l_r & -l_w/2 \\ 1 & +l_r & +l_w/2 \end{pmatrix}\begin{pmatrix} w \\ \eta \\ \phi \end{pmatrix} - \begin{pmatrix} Z_{w1} \\ Z_{w2} \\ Z_{w3} \\ Z_{w4} \end{pmatrix}. \tag{11}$$

A double-acting double-rod hydraulic actuator with symmetric characteristics of both chambers (Fig. 2) is used to generate the active suspension force.

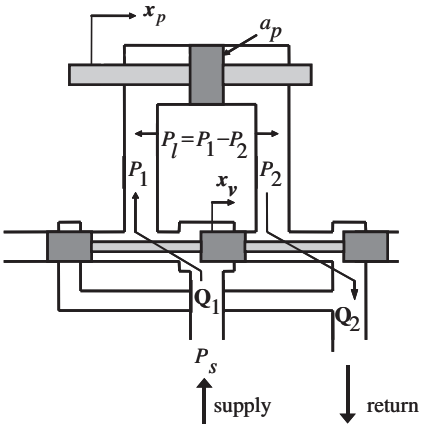

Fig. 2. A double-acting double-rod hydraulic actuator.

The following equations for the actuator load pressure at the vehicle's four corners were used [17]:

$$\dot{P}_{li} = -d_1 P_{li} - d_2 \dot{Z}_{si} + d_3 u_i \sqrt{P_s - \mathrm{sgn}(u_i) P_{li}}, \quad i = 1, 2, \ldots, 4, \tag{12}$$

where the constants d_1, d_2, and d_3 are parameters defined as follows:

$$d_1 = (4\beta_e / V_t) C_{tm}, \quad d_2 = (4\beta_e / V_t) a_p, \quad d_3 = (4\beta_e / V_t) C_d a_d \sqrt{1/\rho}. \tag{13}$$

P_s is the supply pressure of the hydraulic actuator, β_e is the effective bulk modulus, ρ is the working fluid density, V_t is the total volume of actuator cylinder, a_p is the piston area, and C_{tm} and C_d are parameters to be chosen. If $u_i(t)$ is the input signal to the servovalve and $U_i(t)$ is the ith resulting piston force acting on both the sprung and the unsprung masses, it follows that

$$U_i = a_p P_{li}, \quad i = 1, 2, \ldots, 4, \tag{14}$$

In this article, we assume that we have direct control on the input signal to the servovalve, $u_i(t)$, with the dynamics of the servovalve itself being neglected.

3. Suboptimal skyhook damping forces

In this section, we demonstrate the application of a multiple control structure constraint method to obtain optimum skyhook damping forces to be tracked by the nonlinear controllers. The LQG designs have been proven theoretically and experimentally effective at justifying most of the physical insights of all types of active suspensions. However, they cannot be regarded as the only effective way for designing active suspensions as we do not know what other approaches, such as nonlinear programming techniques, might also be applied. Further investigation of this issue in the future would be of great value.

The nonlinear 7-dof model is linearized by neglecting the hydraulic actuator dynamics, including the frictional forces, and by assuming that the active suspension forces are ideally generated. Furthermore, in this linear model, the car is assumed to travel in a constant heading and speed.

A state vector $\mathbf{X}(t)$ of fourteen state variables is considered. It includes seven absolute displacements and seven absolute velocities of the car motion coordinates. The system is described as follows:

$$\dot{\mathbf{X}}(t) = \mathbf{A}\mathbf{X}(t) + \mathbf{B}\mathbf{u}(t) + \mathbf{D}\mathbf{w}(t), \tag{15}$$

$$\mathbf{X}_c(t) = \mathbf{C}\mathbf{X}(t), \tag{16}$$

where $\mathbf{A}$, $\mathbf{B}$, $\mathbf{C}$ and $\mathbf{D}$ are constant matrices of appropriate dimensions. $\mathbf{X}(t)$ is the $(n \times 1)$ state vector, $\mathbf{X}_c(t)$ is the $(n_c \times 1)$ vector of controlled outputs, $\mathbf{u}(t)$ is the $(n_u \times 1)$ control vector, and $\mathbf{w}(t)$ is the $(n_w \times 1)$ disturbance vector of road velocity inputs. In addition, $\mathbf{w}(t)$ is regarded as a vector of Gaussian white noise velocity inputs

imparted at the vehicle tires. For more details on how these road inputs are related to the road roughness and the vehicle heading speed, the reader is referred to Ref. [4].

In a linear quadratic Gaussian control design, the constrained regulator problem solution results in the feedback law [2]:

$$\mathbf{u}(t) = \mathbf{K}\mathbf{X}_m(t), \tag{17}$$

where $\mathbf{K}$ is the $(n_u \times n_m)$ constant feedback matrix and $\mathbf{X}_m(t)$ is the $(n_m \times 1)$ vector of available measurements. The vector of measurable states $\mathbf{X}_m(t)$ is a linear, time-invariant combination of the state vector $\mathbf{X}(t)$. Thus, let

$$\mathbf{X}_m = \mathbf{M}\mathbf{X}, \tag{18}$$

where $\mathbf{M}$ is the $(n_m \times n)$ measurement matrix.

The matrix $\mathbf{K}$ is determined to be the one that minimizes the quadratic criterion

$$J = \lim_{T\to\infty} \frac{1}{T} E\left[\int_0^{\mathrm{T}} [\mathbf{X}_c^{\mathrm{T}} \quad \mathbf{u}^{\mathrm{T}}] \begin{bmatrix} \mathbf{R}_2 & \mathbf{R}_3 \\ \mathbf{R}_3^{\mathrm{T}} & \mathbf{R}_1 \end{bmatrix} \begin{bmatrix} \mathbf{X}_c \\ \mathbf{u} \end{bmatrix} \mathrm{d}t\right], \tag{19}$$

where $\mathbf{R}_1$ is an $(n_u \times n_u)$ positive definite weighting matrix on the control input and $\mathbf{R}_2$ is an $(n_c \times n_c)$ positive semidefinite weighting matrix on the controlled outputs. $\mathbf{R}_3$ is an $(n_c \times n_u)$ weighting matrix that weighs the dynamic coupling between the input control and the controlled outputs. T is the sampling length, and $E[.]$ denotes expected value. The cost function of Eq. (19) is a weighted sum of variances of the input control, the controlled outputs and their dynamic coupling.

Eqs. (17) and (18) imply that $\mathbf{u}(t)$ is a control vector that has a single structure constraint. A multiple control structure constraint problem was originally presented by Kosut [17]. It states that other constraints, rather than the ones defined by Eqs. (17) and (18), are important. Those constraints are: (i) the measurable states that are desirable to use for each control force and (ii) the form or structure that the controller should have. A definition of the problem is stated as follows: Referring to the state variable $\mathbf{X}(t)$ of Eq. (15), if each control force $u_i(t)$, $i = = 1,2,\ldots,n_u$, is constrained to be a linear, time-invariant combination of different sets of measurable states of $\mathbf{X}(t)$, then $\mathbf{u}(t)$ is referred to as a control vector that has a multiple structure constraints.

The mathematical realization of this definition can be achieved by defining the $(n_{mi} \times 1)$ vectors X_{mi}, $n_{mi} \leqslant n$,, for $i = = 1,2,\ldots,n_u$, as a set of vectors whose elements are specified sets of physically measurable states of $\mathbf{X}(t)$. That is,

$$X_{mi} = \mathbf{M}_i X, \quad i = 1, 2, \ldots, n_u, \tag{20}$$

where the $(n_{mi} \times n)$ matrices $\mathbf{M}_i$ will be called the "multiple measurement matrices". In this manner, $u_i(t)$ is a linear combination of the elements of X_{mi}. That is,

$$u_i = \kappa_i^{\mathrm{T}} X_{mi}, \quad i = 1, 2, \ldots, n_u, \tag{21}$$

where κ_i is the ith $(n_{mi} \times 1)$ vector whose elements are the design parameters for control. In other words, the elements of κ_i are the feedback gains of the ith control law $u_i(t)$. If Eqs. (20) and (21) are combined, one gets

$$\mathbf{u}(t) = \mathbf{K}\mathbf{X}(t), \tag{22}$$

where the ith row λ_i of the $(n_u \times n)$ constant feedback matrix $\mathbf{K}$ is given by

$$\lambda_i = \kappa_i^{\mathrm{T}} \mathbf{M}_i, \quad i = 1, 2, \ldots, n_u. \tag{23}$$

The last two equations define the multiple control structure constraint on $\mathbf{u}(t)$ or on $\mathbf{K}$. It is worth noting that, if $n_{mi} = n_m$ and $\mathbf{M}_i = \mathbf{M}$, for all $i = 1, 2, \ldots, n_u$, then the multiple constraints reduce to the single constraint problem. In other words, the multiple control structure constraint is the generalized version of the single control structure constraint.

To this end, it is more convenient to rewrite Eq. (15) as follows:

$$\dot{\mathbf{X}} = \mathbf{A}\mathbf{X} + \sum_{i=1}^{n_u} b_i u_i + \mathbf{D}\mathbf{w}, \tag{24}$$

where b_i is the ith $(n \times l)$ column vector of $\mathbf{B}$ that corresponds to the ith control force $u_i(t)$.

The statement of the (multiple control structure constraint) sub-optimal regulator problem is to find $\mathbf{u}(t)$ that minimizes the cost function in Eq. (19) subjected to the system dynamics in Eqs. (16) and (24) and the multiple control structure constraint defined by Eqs. (20)–(23). Kosut [18] considered the deterministic version of this problem; i.e., the last term in Eq. (24) is ignored and the cost function is considered to be, $(\frac{1}{2})\int_0^\infty(\mathbf{X}^{\mathrm{T}}\mathbf{R}_2\mathbf{X}+\mathbf{u}^{\mathrm{T}}\mathbf{R}_1\mathbf{u})\,\mathrm{d}t$. This treatment is not appropriate for the present problem because our system is stochastically excited by the road surface undulation. Here, we consider the stochastic version of the problem with a generalized cost function as in Eq. (19). Let us define

$$\hat{\mathbf{A}}=\mathbf{A}+\sum_{i=1}^{n_u}b_i\kappa_i^{\mathrm{T}}\mathbf{M}_i=\mathbf{A}+\sum_{i=1}^{n_u}b_i\lambda_i, \tag{25}$$

to be the closed loop matrix. Then, the necessary conditions for the existence of a sub-optimal solution are (proof is in Ref. [3]):

$$\frac{\partial J}{\partial\kappa_i}=2R_{1i}\kappa_i^{\mathrm{T}}\mathbf{M}_i\mathbf{L}_o\mathbf{M}_i^{\mathrm{T}}+2b_i^{\mathrm{T}}\mathbf{L}_c\mathbf{L}_o\mathbf{M}_i^{\mathrm{T}}+2R_{3i}^{\mathrm{T}}\mathbf{C}\mathbf{L}_o\mathbf{M}_i^{\mathrm{T}}=0, \tag{26}$$

$$\kappa_i^{\mathrm{T}}=-\left(\frac{1}{R_{1i}}\right)[b_i^{\mathrm{T}}\mathbf{L}_c\mathbf{L}_o\mathbf{M}_i^{\mathrm{T}}+R_{3i}^{\mathrm{T}}\mathbf{C}\mathbf{L}_o\mathbf{M}_i^{\mathrm{T}}][\mathbf{M}_i\mathbf{L}_o\mathbf{M}_i^{\mathrm{T}}]^{-1}, \tag{27}$$

$$\lambda_i=-\left(\frac{1}{R_{1i}}\right)[b_i^{\mathrm{T}}\mathbf{L}_c\mathbf{L}_o\mathbf{M}_i^{\mathrm{T}}+R_{3i}^{\mathrm{T}}\mathbf{C}\mathbf{L}_o\mathbf{M}_i^{\mathrm{T}}][\mathbf{M}_i\mathbf{L}_o\mathbf{M}_i^{\mathrm{T}}]^{-1}\mathbf{M}_i, \tag{28}$$

$$\hat{\mathbf{A}}\,\mathbf{L}_o+\mathbf{L}_o\hat{\mathbf{A}}^{\mathrm{T}}+\mathbf{D}\mathbf{W}\mathbf{D}^{\mathrm{T}}=0, \tag{29}$$

$$\hat{\mathbf{A}}^{\mathrm{T}}\mathbf{L}_c+\mathbf{L}_c\hat{\mathbf{A}}+\sum_{i=1}^{n_u}\mathbf{M}_i^{\mathrm{T}}\kappa_iR_{3i}^{\mathrm{T}}\mathbf{C}+\sum_{i=1}^{n_u}\mathbf{C}^{\mathrm{T}}R_{3i}\kappa_i^{\mathrm{T}}\mathbf{M}_i+\sum_{i=1}^{n_u}\mathbf{M}_i^{\mathrm{T}}\kappa_iR_{1i}\kappa_i^{\mathrm{T}}\mathbf{M}_i+\mathbf{C}^{\mathrm{T}}\mathbf{R}_2\mathbf{C}=0, \tag{30}$$

and the optimal cost function is calculated by

$$J^*=\mathrm{tr}\left[\mathbf{L}_c\mathbf{D}\mathbf{W}\mathbf{D}^{\mathrm{T}}\right]=\mathrm{tr}\left[\left(\sum_{i=1}^{n_u}\mathbf{M}_i^{\mathrm{T}}\kappa_iR_{3i}^{\mathrm{T}}\mathbf{C}+\sum_{i=1}^{n_u}\mathbf{C}^{\mathrm{T}}R_{3i}\kappa_i^{\mathrm{T}}\mathbf{M}_i+\sum_{i=1}^{n_u}\mathbf{M}_i^{\mathrm{T}}\kappa_iR_{1i}\kappa_i^{\mathrm{T}}\mathbf{M}+\mathbf{C}^{\mathrm{T}}\mathbf{R}_2\mathbf{C}\right)\mathbf{L}_o\right], \tag{31}$$

where tr denotes a matrix trace, which can be considered the algebraic sum of the elements on the diagonal of the matrix $\mathbf{L}_c\mathbf{D}\mathbf{W}\mathbf{D}^{\mathrm{T}}$. R_{1i} is the ith weighting element in the diagonal weighting matrix $\mathbf{R}_1$ that corresponds to the ith control law, and R_{3i} is the ith column in the weighting matrix $\mathbf{R}_3$ that corresponds to the ith control law. A generalized algorithm for solving the problem is summarized in Ref. [2].

4. Global control strategy

In order for each hydraulic actuator to provide exact and instant control forces, it must account for frictional forces. Thus, we need to know the friction forces even in cases of system "lock-up", i.e., when the piston velocity is zero and the friction force is greater than the isolation force.

The approximated friction forces for each actuator would be accepted in the following simple form:

$$F_{fi}=F_{oi}\,\mathrm{sgn}(Z_{bi}-Z_{wi}),\quad i=1,2,\ldots,n_u, \tag{32}$$

where F_{oi}, $i=1,\ldots,n_u$ is the ith amplitude of the actuator frictional force vector $\mathbf{F}_o$. The overall desired hydraulic actuator forces are considered as follows:

$$U_{i_{\mathrm{des}}}=U_{i_{\mathrm{ref}}}+F_{fi},\quad i=1,2,\ldots,n_u, \tag{33}$$

where $U_{i_{\mathrm{des}}}$, is the ith desired actuator force, and, $U_{i_{\mathrm{ref}}}$, is the ith reference actuator force to be tracked. In Ref. [6], it has been suggested to use the "skyhook" damping of sprung mass as a reference actuator force in situations when superior ride quality is desired. Our approach for finding an appropriate reference actuator force benefits from the multiple control structure constraint method of the preceding section in order to

optimize the skyhook damping forces for each actuator. The last section's procedure is implemented, and the measurement matrices are chosen such that the resulting, optimized suspension forces will be

$$U_i = G_{1i}Z_{si} + G_{2i}\dot{Z}_{bi} + G_{3i}\dot{Z}_{wi}, \quad i = 1, 2, ..., n_u, \tag{34}$$

where G_{1i},G_{2i}, and G_{3i}, $i = 1,\ldots,n_u$, are constant feedback gains representing the elements of the $(n_{mi} \times 1)$ optimized gain vector κ_i, $i = 1,\ldots,n_u$. Strictly speaking, the elements of κ_i are the constant feedback gains of the ith control (force) law $u_i(t)$.

Without loss of generality, the ideal control forces in Eq. (34) can be rewritten as follows:

$$U_i = G_{1i}Z_{si} + G_{3i}\dot{Z}_{si} + \tilde{G}_{2i}\dot{Z}_{bi}, \quad i = 1, 2, \ldots, n_u, \tag{35}$$

where $G_{2i} = \tilde{G}_{2i} + G_{3i}$ is performed for each actuator force. It is obvious in Eq. (35) that the first and the second terms on the right-hand side of the equation can be realized by the use of passive means, e.g., a passive spring and dashpot. This means that a part of each control force can be realized by passive isolation elements, and the remaining part, i.e., the skyhook damping forces, is the active (desired) actuator force. In this manner, the reference skyhook actuating forces are

$$U_{i_{\text{ref}}} = \tilde{G}_{2i}\dot{Z}_{bi}, \tag{36}$$

Eq. (36) suggests the use of sub-optimal, collocated skyhook damping forces derived by the structured LQG of Section 3 and the above global control strategy. These forces, if not optimal, might lead to a difficult situation where we have to assume values for these forces, which justify the ride quality measures, the suspension travel and the magnitude of generated skyhook damping forces. If the LQG designs are not to be used, the designer should look for substitutes that provide systematic resolution to the inevitable conflict between performance measures in vehicle suspension designs.

ElBeheiry and Karnopp [2] investigated and compared the performance potentials of various types of collocated and non-collocated active suspension forces. They proved that only collocated forces have a significant impact on the performance potentials by using limited-state LQG design techniques. This proof motivated the collocated skyhook control strategy in this work.

5. Input–output nonlinear controller design

First, let us define a state variable vector of twenty state variables as follows:

$$\mathbf{x} = (Z_{s1}\ Z_{s2}\ Z_{s3}\ Z_{s4}\ Z_{t1}\ Z_{t2}\ Z_{t3}\ Z_{t4}\ \dot{Z}_{b1}\ \dot{Z}_{b2}\ \dot{Z}_{b3}\ \dot{Z}_{b4}\ \dot{Z}_{w1}\ \dot{Z}_{w2}\ \dot{Z}_{w3}\ \dot{Z}_{w4}\ P_{l1}\ P_{l2}\ P_{l3}\ P_{l4}). \tag{37}$$

Differentiating the last equation and substituting from Eqs. (1)–(12), one can formulate the nonlinear system in the following mathematical form [19]:

$$\dot{\mathbf{x}}(t) = \mathbf{f}(\mathbf{x}(t)) + \sum_{i=1}^{n_u} g_i(\mathbf{x}(t))u_i(t) + \mathbf{d}_1\mathbf{F}_f(t) + \mathbf{d}_2\mathbf{w}_r(t) \tag{38}$$

with controlled outputs defined as follows:

$$\mathbf{y}(t) = \begin{pmatrix} y_1(\mathbf{x}(t)) = h_1(\mathbf{x}(t)) \\ \vdots \\ y_{n_y}(\mathbf{x}(t)) = h_{n_y}(\mathbf{x}(t)) \end{pmatrix}, \tag{39}$$

where $\mathbf{x}(t)$ is n-dimensional plant state vector, u_i, $i = 1,\ldots,n_u$, are n_u scalar control inputs, $y_i(t)$, $i = 1,\ldots,n_y$ are n_y scalar plant outputs, $\mathbf{f}(\mathbf{x}), g_1(\mathbf{x}), \ldots, g_{n_u}(\mathbf{x})$, are nonlinear smooth vector fields, and $h_1(\mathbf{x}), \ldots, h_{n_y}(\mathbf{x})$, are smooth functions. $\mathbf{d}_1$ and $\mathbf{d}_2$ are distribution vectors that mathematically locate the suspension frictional forces and the road velocity inputs in their correct positions in the state-space representation, respectively. $\mathbf{F}_f$ is a vector of friction forces, and $\mathbf{w}_r(t)$ is a vector of road velocity inputs. A smooth function refers to a function that is infinitely differentiable.

For our system, we consider the controlled outputs to be the piston (active) forces exerted by the four hydraulic actuators; that is

$$\mathbf{y}_i(t) = a_p P_{li}(t) + F_{fi}(t), \quad i = 1, 2, \ldots, n_u. \tag{40}$$

The idea of the input–output linearization method is based on rendering the output dynamics in the form

$$\begin{bmatrix} y_1^{(r_1)}(t) \\ y_2^{(r_2)}(t) \\ \vdots \\ y_{n_y}^{(r_{n_y})}(t) \end{bmatrix} = \begin{bmatrix} v_1(t) \\ v_2(t) \\ \vdots \\ v_{n_y}(t) \end{bmatrix} \quad \text{or} \quad \mathbf{Y}^{(r)}(t) = \mathbf{v}(t), \quad t \in \Gamma, \tag{41}$$

where Γ is an open time interval containing the point of analysis 0, $r = r_1 + r_2 + \cdots\cdots + r_{n_y}$ is the total relative degree of the system, and r_i is the ith relative degree of the ith controlled output. The relative degree of an output is the number of its differentiations required in order to make the control input appear in the output [19]. Therefore, the statement of the multi-input multi-output linearization problem is to find the constants $r_1, \ldots\ldots, r_{n_y}$ and the static or regular state feedback control law in the form of an inversion-based control law:

$$\mathbf{u}(t) = \mathbf{D}^{-1}(\mathbf{x}(t))(\mathbf{v}(t) - \mathbf{E}(\mathbf{x}(t))), \tag{42}$$

where

$$\mathbf{E}(\mathbf{x}(t)) = \begin{bmatrix} L_f^{r_1} h_1(\mathbf{x}(t)) \\ L_f^{r_2} h_2(\mathbf{x}(t)) \\ \vdots \\ L_f^{r_{n_y}} h_{n_y}(\mathbf{x}(t)) \end{bmatrix}, \quad \mathbf{D}(\mathbf{x}(t)) = \begin{bmatrix} L_{g1} L_f^{r_1 - 1} h_1(\mathbf{x}(t)), \ldots\ldots, L_{gn_y} L_f^{r_1 - 1} h_1(\mathbf{x}(t)) \\ L_{g1} L_f^{r_2 - 1} h_2(\mathbf{x}(t)), \ldots\ldots, L_{gn_y} L_f^{r_2 - 1} h_2(\mathbf{x}(t)) \\ \vdots \\ L_{g1} L_f^{r_{n_y} - 1} h_1(\mathbf{x}(t)), \ldots\ldots, L_{gn_y} L_f^{r_{n_y} - 1} h_{n_y}(\mathbf{x}(t)) \end{bmatrix}. \tag{43}$$

Note that, in the last equation the matrix, $\mathbf{D}(\mathbf{x}(t))$ must be invertible at $\mathbf{x} = \mathbf{x}_o$. $L_f\mathbf{h} = \nabla h.\mathbf{f}$ is called the *Lie Derivative* of $\mathbf{h}$ with respect to $\mathbf{f}$, or, the *directional derivative* of $\mathbf{h}$ along the direction of the vector field f, while $L_g L_f \mathbf{h} = \nabla(L_f \mathbf{h})\mathbf{g}$. It is worth noting that the control law of Eq. (42) is only applicable to the case of square nonlinear system in which the number of outputs equals the number inputs.

The inversion-based control law (42) is not directly applicable to the nonlinear model (38). This is attributed to the existence of the last two terms on the right-hand side of Eq. (42). One term, $\mathbf{d}_1\mathbf{F}_f$, is due to the frictional forces, while the other term, $\mathbf{d}_2\mathbf{w}_r(t)$, is due to the road velocity inputs. As a matter of fact, it is impossible to separate the frictional force from the nonfrictional forces in hydraulic actuators. One idea is to include the frictional forces in the controlled outputs. This assumes a perfect knowledge of the friction magnitudes and their direction signs. In such a case, the actuator would be capable of either cancelling these forces or compensating for them. This would essentially reduce Eq. (33) to

$$U_{i_{\text{des}}} = U_{i_{\text{ref}}} = \tilde{G}_{2i} Z_{bi}. \tag{44}$$

To this end, the inversion-based control law is still not applicable to our model because of the disturbance term, $\mathbf{d}_2\mathbf{w}_r(t)$, which contains the road velocity input. To circumvent such a problem, we exploit the following general result as presented in Ref. [20]:

For a nonlinear system in the form of Eq. (38) and (39) where the term $\mathbf{d}_1\mathbf{F}_f$ vanishes, there exists a feedback of the form of Eq. (42) that renders the output, $y(t)$, independent of the disturbance, $\mathbf{w}_r(t)$, if and only if,

$$L_d L_f^k h_i(t) = 0 \quad \text{for all } 0 \leqslant k \geqslant r_{i-1}, \quad 0 \leqslant i \geqslant n_y. \tag{45}$$

By inspection, it can be easily shown that our model dynamics satisfy this condition. Hence, the inversion-based control law can be calculated by applying the above design procedure

$$u_i(t) = \frac{v_i(t) + a_p d_1 P_{li} + a_p d_2 \dot{Z}_{si}}{a_p d_3 \sqrt{P_s - P_{li}\,\text{sgn}(u_i)}}, \quad i = 1, 2, \ldots, n_u. \tag{46}$$

The zero dynamics remain to be investigated. Since the order of the system is 20 and the total relative degree is 4, we define a 16-dimensional autonomous subsystem called zero dynamics. This system determines whether the control laws (46) are capable of locally stabilizing the closed loop dynamics or not. Actually, instead of checking the internal stability of the system by using its normal forms [21], one can follow a simpler method that depends on the special form of our system. The system is in its controllability canonical form, meaning that, if we can get the exogenous part of the input control, $\mathbf{v}(t)$, to stabilize the (controlled outputs) nonlinear part of the system, it follows that the whole system will be stable.

If each component of the output $y_i(t)$ asymptotically tracks a scalar reference input, $y_{di}(t)$, then the exogenous part of the input control law, $\mathbf{v}(t)$, can be chosen as follows:

$$v_i = y_{di}^{(r_i)} - k_{i(r_i-1)}e_i^{(r_i-1)} - \cdots\cdots\cdots - k_{i1}e_i^{(1)} - k_{oi}e_i, \quad i = 1,\ldots,n_y, \tag{47}$$

where

$$e_i(t) = y_i(t) - y_{di}(t), \tag{48}$$

gives

$$e_i^{(r_i)} + k_{i(r_i-1)}e_i^{(r_i-1)} + \cdots\cdots\cdots + k_{i1}e_i^{(1)} + k_{oi}e_i = 0, \quad i = 1,\ldots,n_y. \tag{49}$$

The ability of the system to track desired outputs and even its own stability will be controlled by the appropriate selection of the constants $k_{i(ri-1)},\ldots,k_{oi}$, $i = 1,\ldots,n_y$. Following the asymptotic tracking procedure (47), the exogenous control input, $\mathbf{v}(t)$, can be designed. Hence, by differentiating Eq. (40), with the friction term temporarily neglected, one obtains the derivatives of the controlled outputs to be in the following linearized form:

$$\dot{y}_i = \frac{1}{a_p}(\tilde{G}_{2i}\ddot{Z}_{bi} - K_{oi}(a_pP_{li} - \tilde{G}_{2i}\dot{Z}_{bi})), \quad i = 1,2,\ldots,n_y. \tag{50}$$

6. Sliding mode controller design

The statement of the sliding control problem is to get the state $\mathbf{x}(t)$ to track a specific time-varying desired state $\mathbf{x}_d(t) = (x_d, x_d^{(1)},\ldots\ldots\ldots, x_d^{(n-1)})^{\mathrm{T}}$ in the presence of model uncertainties on the plant and control gain functions $\mathbf{f}(\mathbf{x}(t))$ and $\mathbf{g}(\mathbf{x}(t))$, respectively. If a MIMO system has a vector relative degree $[r_1,\ldots\ldots\ldots,r_{n_y}]$, then the statement of the MIMO sliding mode control problem is to find an n_y sliding surfaces [20]:

$$s_i(t) = e_i^{(r_i-1)} + k_{i(r_i-1)}e_i^{(r_i-2)} + \cdots\cdots\cdots + k_{i2}e_i^{(1)} + k_{i1}e_i + k_{i0}\int e_i\,\mathrm{d}t = 0, \tag{51}$$

such that a control input vector $\mathbf{u}$ fulfills sliding conditions of the form [19]:

$$\frac{1}{2}\frac{\mathrm{d}}{\mathrm{d}t}s_i^2(t) \leqslant -\xi_i|s_i(t)|, \quad \xi_i > 0, \tag{52}$$

where ξ_i, $i = 1,\ldots\ldots,n_y$, are positive numbers. A control law can be designed for achieving the sliding surfaces by first solving for $\mathbf{u}$ from the following condition:

$$\dot{\mathbf{s}}(t) = \begin{bmatrix} \dot{s}_1(t) \\ \vdots \\ \dot{s}_{n_y}(t) \end{bmatrix} = \mathbf{v}(t). \tag{53}$$

By letting

$$v_i(t) = -k_{vi}\,\mathrm{sgn}(s_i(t)), \tag{54}$$

where k_{vi} is a positive number greater than the positive number ξ_i, the sliding conditions are fulfilled. The control law can be written as [19]:

$$\mathbf{u}(t) = \mathbf{D}^{-1}(\mathbf{x}(t))(-\mathbf{Y}^{(r-1)}(t) - \mathbf{E}(\mathbf{x}(t)) - \mathbf{k}_v \operatorname{sgn}(\mathbf{s}(t))). \tag{55}$$

Under some kinds of uncertainties, it is easy to show that by appropriate selection of the values k_{vi}, $i = 1,\ldots,n_y$, the sliding conditions can be satisfied.

Taking into consideration that the relative degree for each controlled output is one, and according to Eq. (50), we choose the sliding surfaces for the controllers such that:

$$s_i = a_p P_{li} - U_{i_{des}}, \quad i = 1, 2, \ldots, n_u. \tag{56}$$

The sliding manifold can be made attractive by choosing control laws to satisfy condition (52). However, to ensure that the controlled output tracks the desired force exponentially, we set:

$$\dot{s}_i = (a_p \dot{P}_{li} - \dot{U}_{i_{des}}) = -k_{i1}(a_p P_{li} - U_{i_{des}}), \quad i = 1, \ldots, n_u. \tag{57}$$

Following the above procedure, the control inputs can be calculated as follows:

$$u_i = \frac{\dot{U}_{i_{\mathrm{des}}} + k_{i1} U_{i_{\mathrm{des}}} + a_p(\hat{d}_1 - k_{i1})P_{li} + a_p \hat{d}_2 \dot{Z}_{si} - k_{vi} \operatorname{sgn}(s_i)}{a_p \hat{d}_3 \sqrt{P_s - P_{li} \operatorname{sgn}(u_i)}}, \quad i = 1, 2, \ldots, n_u, \tag{58}$$

where $\hat{d}_1, \hat{d}_2$, and $\hat{d}_3$ are the model estimates of d_1,d_2, and d_3, respectively. It is assumed here that the uncertainties are additive and that they are upper-bounded such that [22]:

$$d_j = \hat{d}_j + \Delta d_j \quad \text{and} \quad |\Delta d_j| < \Delta D_j, \quad j = 1, 2, 3. \tag{59}$$

The robustness parameters, k_{vi}, $i = 1,2,\ldots,n_u$, can satisfy the attraction condition in Eq. (54) if the following conditions holds true:

$$k_{vi} > \Delta D_1 + \Delta D_2 + \Delta D_3, \quad i = 1, 2, \ldots, n_u. \tag{60}$$

In practice, the induced chatter due to the use of sgn(**s**) in the control laws (58) is undesirable based on the possibility of exciting unmodelled high frequency dynamics. To deal with such a problem, we use a saturation function sat(**s**/ϖ) [21] such that:

$$\operatorname{sat}(s_i/\varpi_i) = \begin{cases} \operatorname{sgn}(s_i) & |s_i| > \varpi_i, \\ (s_i/\varpi_i) & |s_i| < \varpi_i, \end{cases} \quad i = 1, \ldots, n_u, \tag{61}$$

where ϖ is the boundary layer thickness and may be used to achieve the robustness. The boundary layer thickness ϖ, the control constants k_{i1}, $i = 1,\ldots,n_u$ and the robustness parameters can be chosen to satisfy [22]:

$$\varpi_i \geqslant (k_{vi}/k_{i1}), \quad i = 1, \ldots, n_u. \tag{62}$$

However, by judiciously selecting the robustness parameters and the boundary layer thickness, desired tracking performance can be guaranteed, while eliminating or substantially reducing chatter.

7. Results and discussions

It is worth noting that all computations for this studied were performed on a Matlab/simulink-based program VEHDYN5 developed by the author for the dynamic analysis and suspension design of ground vehicles. The numerical example begins with the application of the multiple control structure constraint method to the linearized system model of Eqs. (15)–(18) as described in Section 4. The aim is to obtain both the optimal skyhook damping forces and the optimal passive suspension elements. The optimal skyhook damping forces are to be tracked by the hydraulic actuators, and the optimal passive suspension elements are to be mechanized in parallel with the hydraulic actuators in order to increase the system reliability. The numerical values of the vehicle model and the actuator parameters are shown in Tables 1 and 2, respectively.

The multiple control structure constraints method starts with the selection of the weighting matrices in the quadratic performance index (19). Since we have four control inputs, seven controlled outputs, which are the displacements of sprung and unsprung masses, and no passive elements, the weighting matrices are chosen as

Table 1
Basic car model parameter values

Parameter	Value	Parameter	Value
m_s	1460 kg	k_{s1},k_{s2}	To be designed
I_x	460 kg m^2	k_{s3},k_{s4}	–
I_y	2460 kg m^2	c_{s1},c_{s2}	–
m_{w1},m_{w2}	40 kg	c_{s3},c_{s4}	–
m_{w3},m_{w4}	35.5 kg	k_{t1},k_{t2},k_{t3},k_{t4}	175 500 N/m
l_w	1.5 m	l_f	1.0 m
l_r	1.8 m		

Table 2
Hydraulic actuator parameter values

a_p (m^2)	P_s (Pa)	d_1	d_2 (N/m^3)	d_3 (N(m$^{5/2}$kg$^{1/2}$))
3.35×10^{-4}	10342500	1	4.528746×10^{9}	1.545×10^{9}

follows:

$$\mathbf{R}_1=\begin{bmatrix}5\times10^{-8} & 0 & 0 & 0\\ 0 & 5\times10^{-8} & 0 & 0\\ 0 & 0 & 5\times10^{-8} & 0\\ 0 & 0 & 0 & 5\times10^{-8}\end{bmatrix},$$

$$\mathbf{R}_2=\begin{bmatrix}40&0&0&0&0&0&0\\0&40&0&0&0&0&0\\0&0&40&0&0&0&0\\0&0&0&30&0&0&0\\0&0&0&0&30&0&0\\0&0&0&0&0&30&0\\0&0&0&0&0&0&30\end{bmatrix},$$

$$\mathbf{R}_3=[0]. \tag{63}$$

In order to get solutions in the form of Eq. (33), the following measurement matrices are designed:

$$\mathbf{M}_1=\begin{bmatrix}1&l_f&l_w/2&-1&0&0&0&0&0&0&0&0&0&0\\0&0&0&0&0&0&0&1&l_f&l_w/2&0&0&0&0\\0&0&0&0&0&0&0&0&0&0&1&0&0&0\end{bmatrix},$$

$$\mathbf{M}_2=\begin{bmatrix}1&l_f&-l_w/2&0&-1&0&0&0&0&0&0&0&0&0\\0&0&0&0&0&0&0&1&l_f&-l_w/2&0&0&0&0\\0&0&0&0&0&0&0&0&0&0&0&1&0&0\end{bmatrix},$$

$$\mathbf{M}_3=\begin{bmatrix}1&-l_r&l_w/2&0&0&-1&0&0&0&0&0&0&0&0\\0&0&0&0&0&0&0&1&-l_r&l_w/2&0&0&0&0\\0&0&0&0&0&0&0&0&0&0&0&0&1&0\end{bmatrix},$$

$$\mathbf{M}_4 = \begin{bmatrix} 1 & -l_r & -l_w/2 & 0 & 0 & 0 & -1 & 0 & 0 & 0 & 0 & 0 & 0 & 0 \\ 0 & 0 & 0 & 0 & 0 & 0 & 0 & 1 & -l_r & -l_w/2 & 0 & 0 & 0 & 0 \\ 0 & 0 & 0 & 0 & 0 & 0 & 0 & 0 & 0 & 0 & 0 & 0 & 0 & 1 \end{bmatrix}. \tag{64}$$

Any of the unconstrained optimization algorithms in the Matlab/Optimization toolbox can be implemented for solving the suboptimal LQG problem. This requires a consecutive solution of the two Lyapunov matrix Eqs. (29) and (30) in each iteration in order to minimize the performance index (31). However, there is no guarantee that the attainable solutions are stable. Many iterations might be required to adjust the parameters of the weighting matrices before the designer can get a solution that is stable and satisfactory. Theoretically, the problem has a very large number of solutions, only a few of which fulfill all of the designer's desires. According to Eq. (34), the following solution is one that was found to be effective at resolving the inevitable conflict among the many performance measures of suspension system design:

$$\begin{aligned} U_1 &= 26313Z_{s1} + 3829\dot{Z}_{b1} - 973\dot{Z}_{w1}, \\ U_2 &= 26313Z_{s2} + 3829\dot{Z}_{b2} - 973\dot{Z}_{w2}, \\ U_3 &= 24157Z_{s3} + 3293\dot{Z}_{b3} - 930\dot{Z}_{w3}, \\ U_4 &= 24157Z_{s4} + 3293\dot{Z}_{b4} - 930\dot{Z}_{w4}. \end{aligned} \tag{65}$$

Following the design procedure of Eqs. (35) and (36), the sub-optimal passive spring and dashpot constants at the front and rear suspensions can be calculated as follows:

$$\begin{aligned} k_{s1} &= k_{s2} = 26\,313\ \mathrm{N/m}, \\ c_{s1} &= c_{s2} = 994\ \mathrm{N\,s/m}, \\ k_{s3} &= k_{s4} = 24\,157\ \mathrm{N/m}, \\ c_{s3} &= c_{s4} = 930\ \mathrm{N\,s/m}, \end{aligned} \tag{66}$$

and the desired skyhook damping forces will be

$$\begin{aligned} U_{1_{\mathrm{des}}} &= 2835\dot{Z}_{b1}, \\ U_{2_{\mathrm{des}}} &= 2835\dot{Z}_{b2}, \\ U_{3_{\mathrm{des}}} &= 2501\dot{Z}_{b3}, \\ U_{4_{\mathrm{des}}} &= 2501\dot{Z}_{b4}. \end{aligned} \tag{67}$$

According to the design procedure outlined in Section 5, it is obvious that the input–output controller is capable of stabilizing the system for any positive values of the tracking coefficients k_{oi}, $i = 1,2,\ldots,n_u$ of Eq. (49). In other words, since the ith relative degree is only one, Eq. (49) simplifies to $k_{oi}e_i = 0$, $i = 1,2,\ldots,n_u$ Therefore, only the tracking coefficients k_{oi}, $i = 1,2,\ldots,n_u$ will influence the system's tracking ability as well as its own stability. These coefficients were assigned the following values: $k_{o1} = k_{o2} = 275$ and $k_{o3} = k_{o4} = 375$.

For a vehicle heading at a constant speed of 50 km/h and subjected to a harmonic road velocity input of 2 cm amplitude, Fig. 3 shows that the input–output controller is capable of tracking the desired damping forces in absence of the coulomb friction forces and the model uncertainties.

Instead of using the simplified friction model that was introduced in Eq. (32), we used a more realistic and easy-to-implement "stick-slip" friction model as presented in Ref. [23]. Such a model not only allows the computation of the frictional forces during the sticking and slipping motions, but it also considers the problem of integration algorithm stability associated with near-zero velocity force computations. Fig. 4 depicts the behavior of the input–output controller in the presence of friction. It can be easily deduced that this controller is incapable of dealing with the friction forces due to the pulses that appear at the instant of sticking friction, i.e., at the moment when the friction forces change sign and drop to slipping friction magnitudes. In fact, such

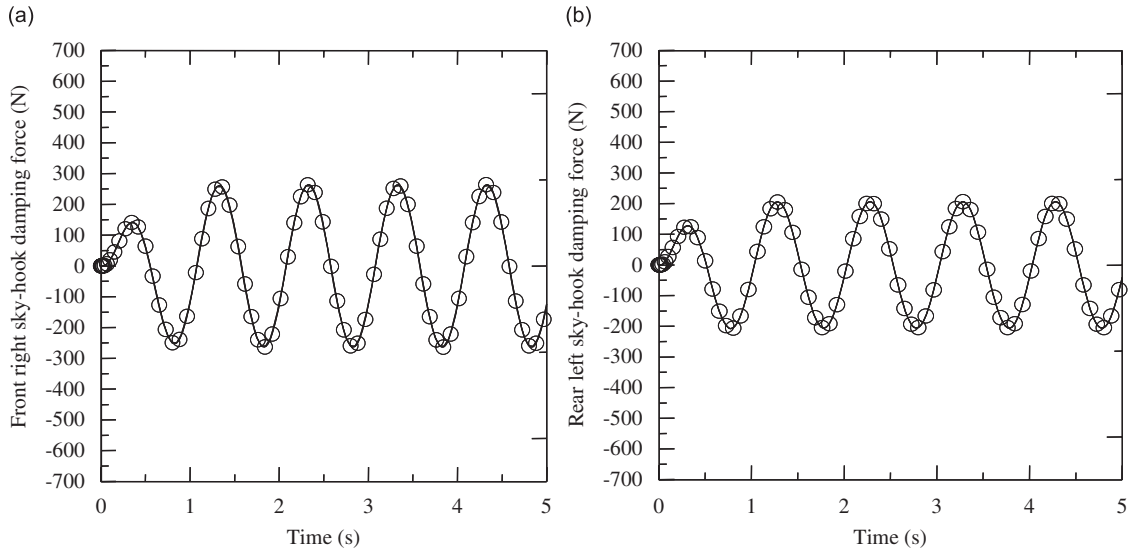

Fig. 3. Skyhook damping force for the input–output controller w/o friction and model uncertainty: (a) front-right corner and (b) rear-left corner. (—) Desired force and (O) actual force.

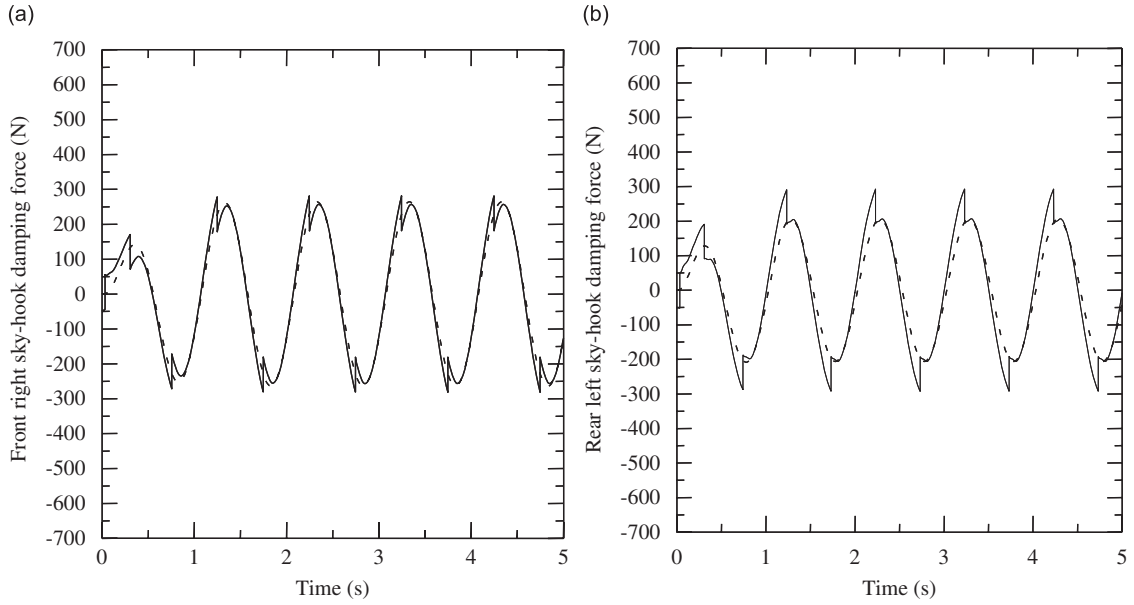

Fig. 4. Skyhook damping force for the input–output controller with friction: (a) front-right corner and (b) rear-left corner. (- -) Desired force and (—) actual force.

pulses do not appear in the output actuator forces due to the very fast dynamics of the spool valves relative to the actuator's own dynamics. This does not necessarily mean the skyhook damping forces will not be affected by such overshoots (Fig. 4). In fact, as there is a continuous cancellation or interaction between these damping forces and the "stick-slip" forces, it was expected that skyhook damping forces would be affected. Consequently, an increase in the sprung mass acceleration is the logical result and ride harshness is inevitable.

Now, the uncertainties of the actuator constants d_1 and d_2 are considered to be 20%, while 30% is considered for the constant d_3. To clarify the effects of model uncertainties on the input–output controller, we temporarily excluded the friction forces from the model. The simulation results are shown in Fig. 5.

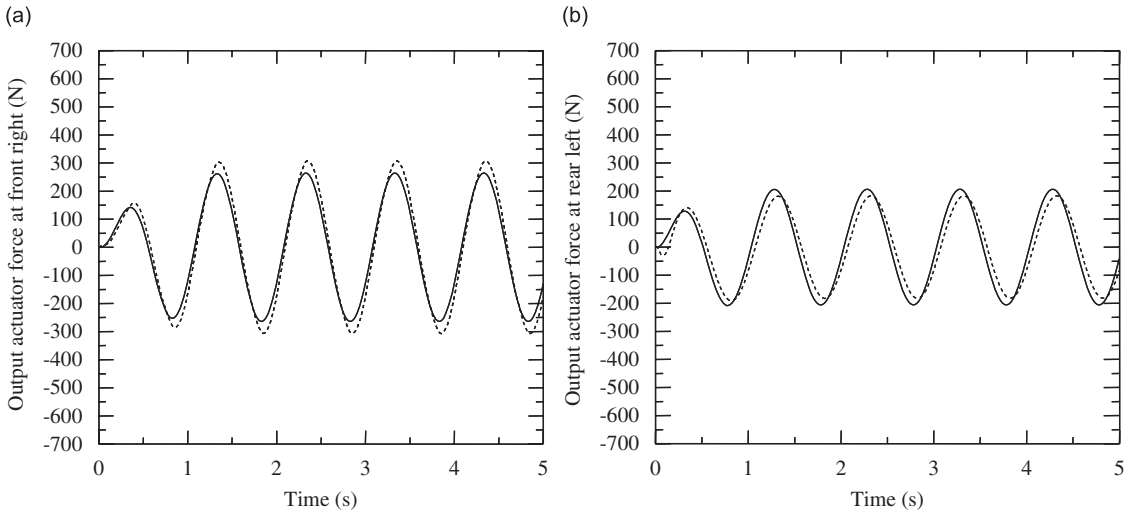

Fig. 5. Output actuator force for the input–output controller with model uncertainty: (a) front-right corner and (b) rear-left corner. (- -) Actual force and (—) desired force.

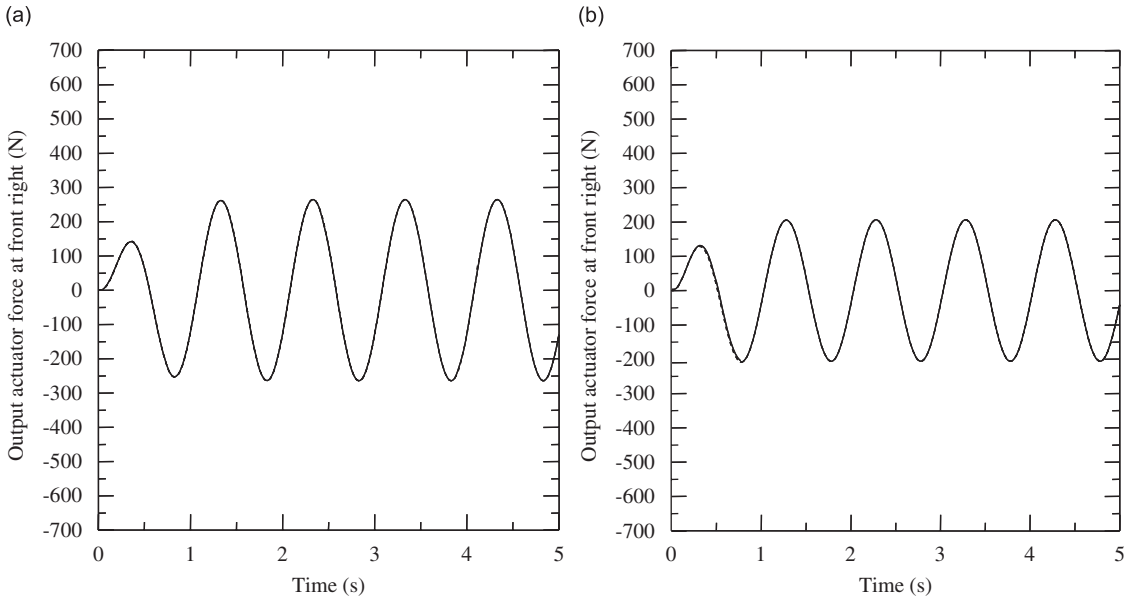

Fig. 6. Output actuator force for the sliding mode controller with model uncertainty: (a) front-right corner and (b) rear-left corner. (- -) Actual force and (—) desired force.

The controller is also incapable of performing satisfactorily. The controller would provide greater output force at one corner (Fig. 5a) and a weaker force at the other (Fig. 5b), but they never coincided with the desired performance.

The simulation results of the sliding mode controller, in the presence of model uncertainty, are presented in Fig. 6. We selected the controller parameters according to Eqs. (51) and (57) such that:

$$k_{11} = k_{21} = 1052,$$

$$k_{31} = k_{41} = 1295. \tag{68}$$

When the model uncertainties exist, the robustness parameters are chosen according to Eqs. (60) such that

$$k_{v1} = k_{v2} = \Delta D_1 + \Delta D_2 + \Delta D_3 + 1000,$$

$$k_{v3} = k_{v4} = \Delta D_1 + \Delta D_2 + \Delta D_3 + 2000. \tag{69}$$

If the model uncertainties do not exist, the robustness parameters become

$$k_{v1} = k_{v2} = 1000,$$

$$k_{v3} = k_{v4} = 2000. \tag{70}$$

Fig. 6 shows that the sliding mode controller is capable of providing excellent (almost exact) tracking even when model errors exist.

It would be helpful for the reader to come to a full understanding of the design procedures presented in the preceding sections if the effects of relaxing the optimality and stability conditions are investigated. Here, a (ramp) half-harmonic road height input of 0.05 m amplitude was imparted at the right front and rear tires with a time delay between them encountered in simulation. Another simultaneous half-harmonic road height input

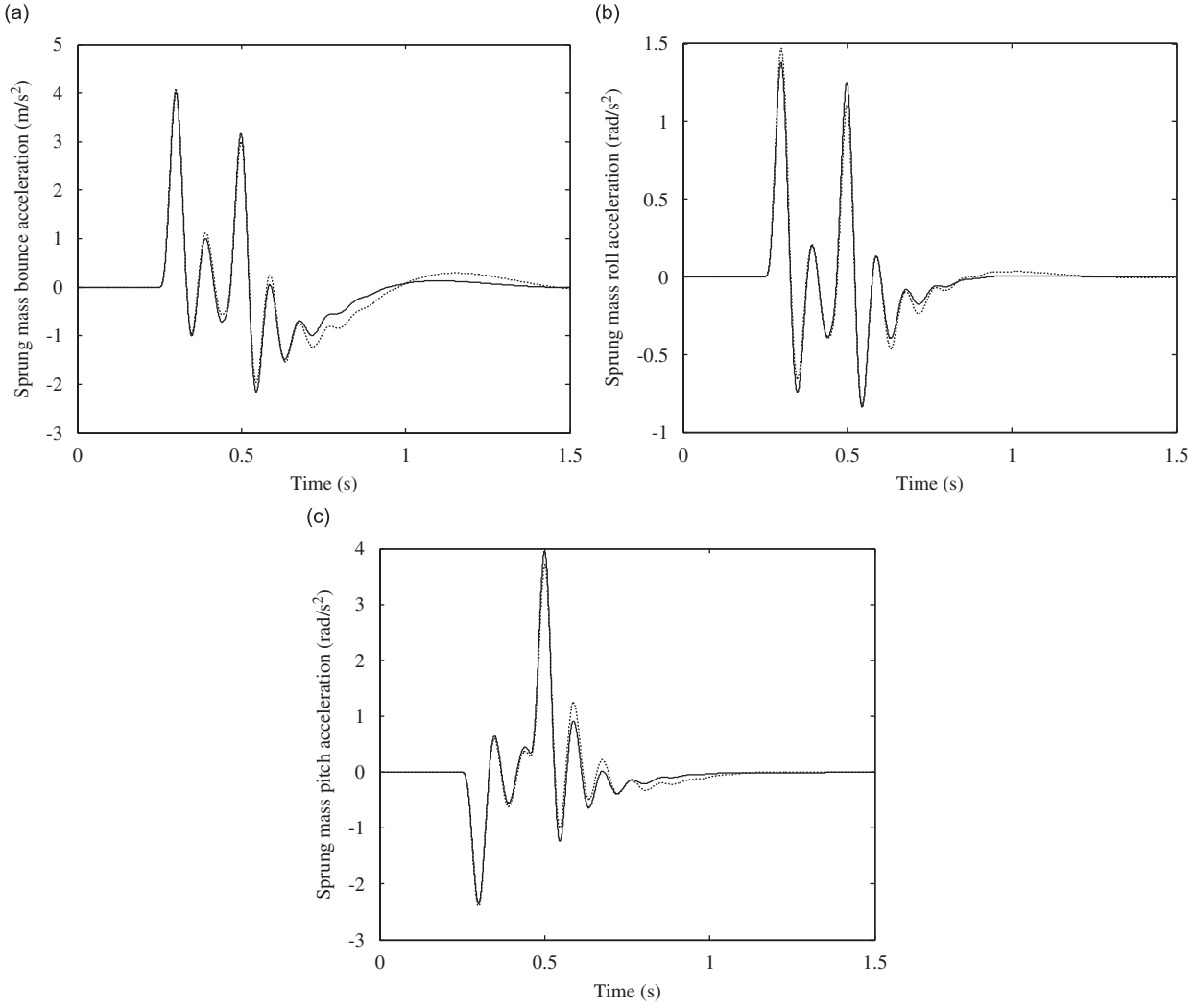

Fig. 7. Sprung mass response for the input–output controller: (a) bounce acceleration, (b) roll acceleration and (c) pitch acceleration. (—) Optimal suspension and skyhook damping and (…) non-optimal suspension and skyhook damping.

of 0.07 m amplitude was imparted at the left front and rear tires with the time delay between them encountered in simulation. The difference in magnitude between the road height inputs at the right and left tires is meant to excite the roll mode of the sprung mass. All the numerical values assigned to the design parameters of the two controllers in the above example are restored for the current investigation. These values represent a design case study of optimal and stable input–output and sliding mode controllers.

For the input–output controller, the effect of optimality on the system design measures is investigated by replacing the optimal solution of Eqs. (65) and (66) by a non-optimal solution, which assigns the following values for the passive suspension elements and the gain of the skyhook damping force:

$$k_{s1} = k_{s2} = 22\,313\ \mathrm{N/m},$$

$$c_{s1} = c_{s2} = 1050\ \mathrm{N\,s/m},$$

$$k_{s3} = k_{s4} = 17\,157\ \mathrm{N/m},$$

$$c_{s3} = c_{s4} = 830\ \mathrm{N\,s/m}, \tag{71}$$

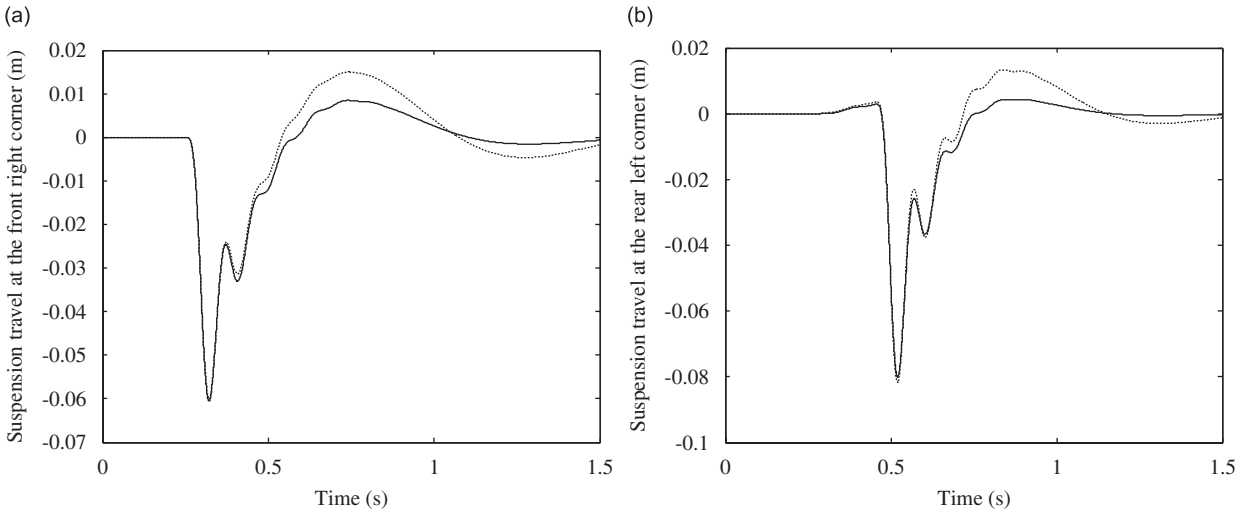

Fig. 8. Suspension travel for the input–output controller: (a) front-right corner and (b) rear-left corner. (—) Optimal suspension and skyhook damping and (…) non-optimal suspension and skyhook damping.

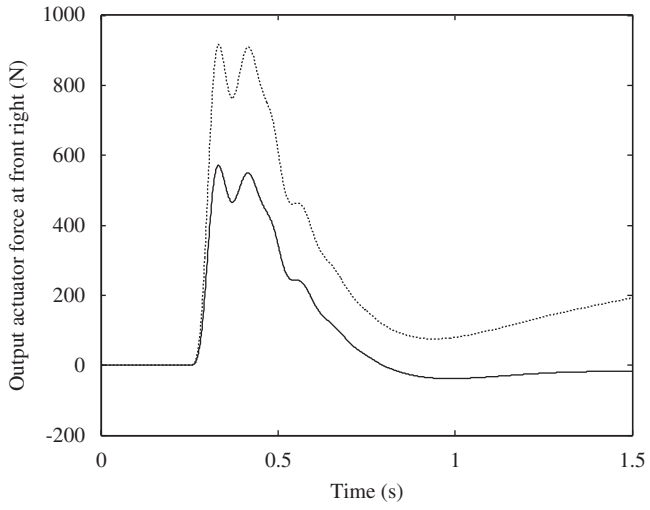

Fig. 9. Output actuator force for the input–output controller: (—) stable design and (…) unstable design.

$$U_{1_{des}} = 1535\dot{Z}_{b1},$$

$$U_{2_{des}} = 1535\dot{Z}_{b2},$$

$$U_{3_{des}} = 1201\dot{Z}_{b3},$$

$$U_{4_{des}} = 1201\dot{Z}_{b4}. \quad (72)$$

Fig. 7 shows the sprung mass bounce, roll and pitch accelerations in response to the road height inputs for the non-optimal solution as compared to the optimal one. The same comparison is made in terms of the suspension travel at the front right and rear left corners of the vehicle as shown in Fig. 8. The two figures reveal that there is a marginal change in the vehicle response if the solution is not optimal. In other words, the optimal solution becomes a steady response faster than the non-optimal solution, and this fact holds true for both the suspension travel and the sprung mass accelerations.

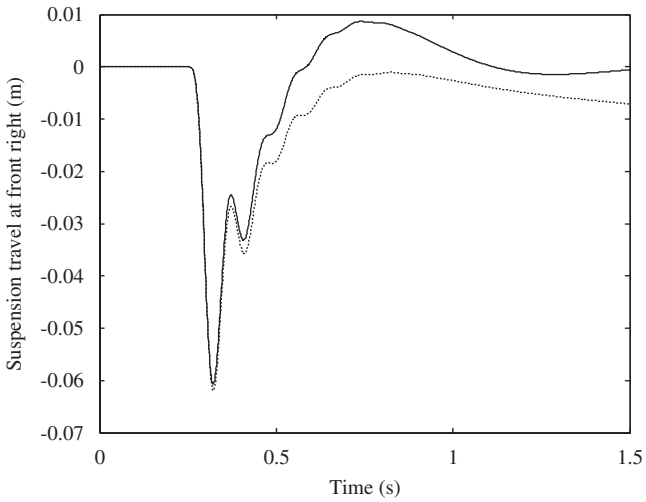

Fig. 10. Suspension travel for the input–output controller: (—) stable design and (…) unstable design.

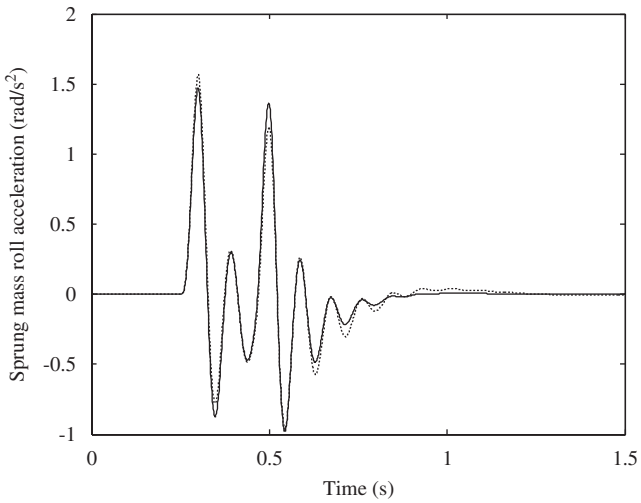

Fig. 11. Sprung mass roll acceleration for the sliding mode controller: (—) optimal suspension and skyhook damping and (…) non-optimal suspension and skyhook damping.

Inappropriate selection of the tracking coefficients could drive the input–output controller to instability. To investigate this issue, we switch back to the optimal passive and skyhook parameter values as presented in Eqs. (66) and (67) with the controller tracking coefficients given the following inappropriate values: $k_{oi} = -1$, $i = 1,2,\ldots,n_u$. These values must drive the system unstable as the positiveness constraint on these tracking coefficients would be violated. Fig. 9 shows that the generated actuator force is incapable of tracking the ideal skyhook damping force due to the system instability. Consequently, the response of the system is significantly deteriorated in response to the road height input as shown in Fig. 10.

The effects of the above investigated issues of non-optimality and instability are repeated for the sliding mode controller. First, the non-optimality effects on this type of controller are investigated. In the absence of model uncertainties, two different simulations are made with the parameter values of the controller in Eqs. (68) and (70) remaining unchanged. The difference is that, in the first simulation, the optimal suspension and skyhook damping parameters in Eqs. (66) and (67) are used, while in the second simulation, the non-optimal parameter values of the suspension and skyhook damping in Eqs. (71) and (72) are used.

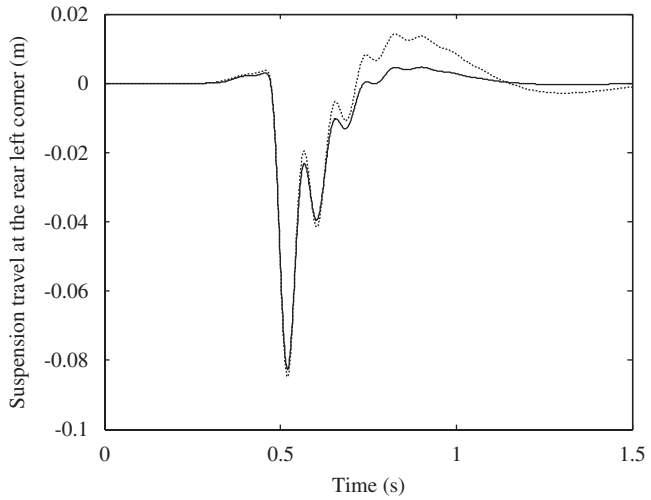

Fig. 12. Suspension travel for the sliding mode controller: (—) optimal suspension and skyhook damping and (…) non-optimal suspension and skyhook damping.

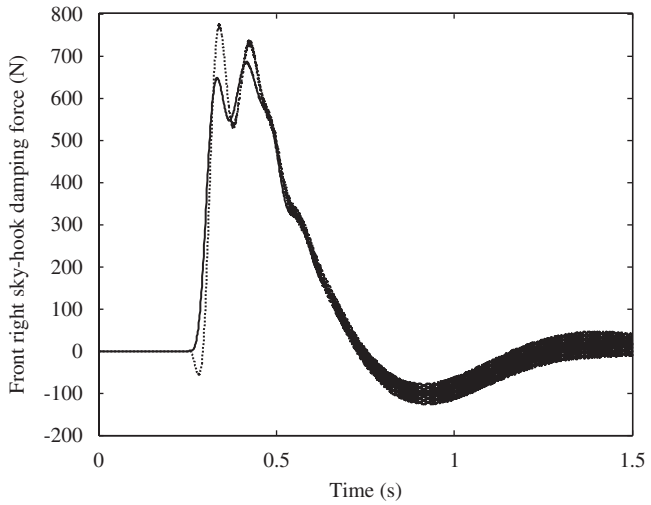

Fig. 13. Output actuator force for the sliding mode controller: (—) stable design and (…) unstable design.

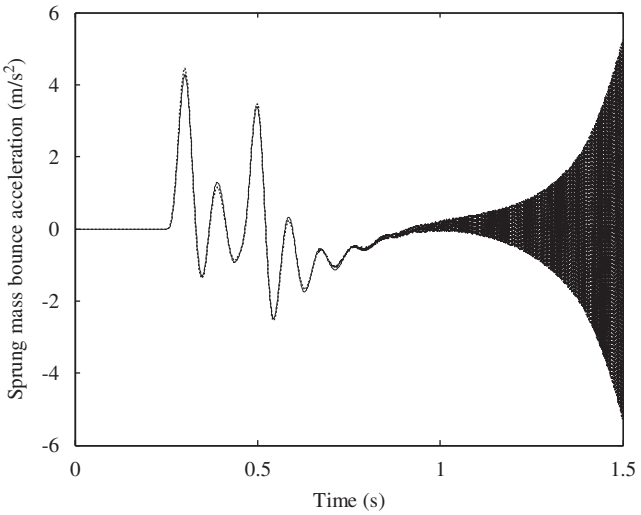

Fig. 14. Sprung mass acceleration for the sliding mode controller: (—) stable design and (…) unstable design.

Figs. 11 and 12 indicate that the optimal solution is still better than the non-optimal one even with the sliding mode controller.

To investigate the effects of inappropriate design or parameter selection for the sliding mode controller, we switched back to the optimal suspension design of the Eqs. (66) and (67). This optimal solution was held unchanged during two different simulations. The controller parameters in Eqs. (68) and (70) also remained unchanged. Note here that the controller parameters of Eqs. (68) and (70) do not account for the model uncertainties. The set of parameters that account for the model uncertainties is in Eq. (69). In the first simulation, model uncertainties are considered zeros, while in the second simulation, uncertainties are introduced into the actuator parameters such that: $\Delta D_1 = 0.2d_1$, $\Delta D_2 = 0.3d_2$, and $\Delta D_3 = 0.2d_3$. Comparisons of the results of the two simulations are shown in Figs. 13 and 14. The inappropriate selection of the tracking gains when uncertainties are introduced into the model led to deterioration of the controller tracking ability as shown in these figures. Response chattering is magnified with time by the sprung mass acceleration and will lead to high ride harshness due to instability and high frequency resonance. The use of the sliding mode parameters in Eq. (69) will absolutely lead to excellent tracking capability and will suppress the chattering.

8. Conclusions

A detailed computational design procedure of active hydraulic suspensions for ground vehicles has been presented. This procedure combines a linear sub-optimal multiple control structure constraints method with nonlinear control design methods in order to achieve the maximum performance potential of hydraulic vehicle suspensions. The method is demonstrated by a numerical example that shows its effectiveness. The simulation results emphasize the suitability of the sliding mode controller in tracking optimal linear desired suspension forces even in cases of model errors and uncertainty. Digital simulation also shows that the use of the input–output controller is significant as long as the suspension is frictionless and the system knowledge is perfect.

References

[1] E.M. ElBeheiry, D.C. Karnopp, M.E. ElAraby, A.M. AbdelRaouf, Advanced ground vehicle suspension systems—a classified bibliography, *Vehicle System Dynamics* 24 (1995) 231–258.

[2] E.M. ElBeheiry, D.C. Karnopp, Optimization of active and passive suspensions based on a full car model, *SAE Special Issue on Progress in Technology* 77 (1995) 341–352.

[3] E.M. ElBeheiry, D.C. Karnopp, M.E. ElAraby, A.M. AbdelRaouf, Suboptimal control design of active and passive suspensions based on a full car model, *Vehicle System Dynamics* 26 (1996) 197–222.
[4] E.M. ElBeheiry, Effects of small travel speed variations on active vibration control in modern vehicle, *Journal of Sound and Vibration* 232 (5) (2000) 857–875.
[5] E.M. ElBeheiry, Y. Zeyada, M.E. ElAraby, Handling capabilities of vehicle in emergencies using coordinated AFS and ARMC systems, *Vehicle System Dynamics* 35 (3) (2001) 195–215.
[6] A. Alleyne, P.D. Neuhaus, J.K. Hedrick, Application of nonlinear control theory to electronically controlled suspensions, *Vehicle System Dynamics* 22 (1993) 309–320.
[7] G.H. Engelman, G. Rizzoni, Including the force generation process in active suspension control formulation, *Proceedings of the 1993 American Control Conference*, 1993, pp. 701–705.
[8] A. Chamseddine, T. Raharijaona, H. Noura, Sliding mode control applied to active suspension using nonlinear full vehicle and actuator dynamics, *Proceedings of the 45th IEEE Conference on Decision and Control*, Vol. 6, 2006, pp. 3597–3602.
[9] A. Alleyne, R. Liu, A simplified approach to force control for electro-hydraulic systems, *Control Engineering Practice* 8 (2000) 1347–1356.
[10] S. Chantranuwathana, H. Peng, Adaptive robust force control for vehicle active suspensions, *International Journal of Adaptive Control and Signal Processing* 18 (2) (2004) 83–102.
[11] P.A. Ioannou, J. Sun, *Robust Adaptive Control*, Prentice-Hall, Englewood Cliffs, NJ, 1996.
[12] L. Zuo, J.-J.E. Slotine, S.A. Nayfeh, Model reaching adaptive control for vibration isolation, *IEEE Transactions on Control Systems Technology* 13 (4) (2005) 611–617.
[13] J. Campos, F.L. Lewis, L. Davis, S. Ikenaga, Backstepping based fuzzy logic control of active vehicle suspension systems, *Proceedings of the American Control Conference*, 2000, pp. 4030–4035.
[14] S.-J. Huang, H.-C. Chao, Fuzzy logic controller for a vehicle active suspension system, *Proceedings of the Institution of Mechanical Engineers, Part D: Journal of Automobile Engineering* 214 (D1) (2000) 1–12.
[15] C. Kaddissi, J.P. Kenne, M. Saad, Drive by wire control of an electro-hydraulic active suspension—a backstepping approach, *IEEE International Conference on Control Applications*, 2005, pp. 1581–1587.
[16] J.-C. Renn, T.-H. Wu, Modeling and control of a new $\frac{1}{4}$T servo-hydraulic vehicle active suspension system, *Journal of Marine Science and Technology* 15 (3) (2007) 265–272.
[17] H.E. Merritt, *Hydraulic Control Systems*, Wiley, New York, 1967.
[18] R.B. Kosut, Suboptimal control of linear time-invariant systems subject to control structure constraints, *IEEE Transactions on Automatic Control* 15 (1970) 557–563.
[19] E. J-J. Slotine, W. Li, *Applied Nonlinear Control*, Prentice-Hall, Inc., Englewood Cliffs, NJ, 1991.
[20] A. Isidori, *Nonlinear Control Systems*, Springer, Berlin, 1985.
[21] C.-F. Lin, *Advanced Control Systems Design*, PTR Prentice-Hall, New Jersey, 1995.
[22] D.D. Cho, Experimental results on sliding mode control of an electromagnetic suspension, *Mechanical Systems and Signal Processing* 7 (4) (1993) 283–292.
[23] D.C. Karnopp, Computer simulation of stick-slip friction in mechanical dynamic systems, *ASME Transactions—Journal of dynamic Systems, Measurements, and Control* 107 (1985) 100–103.